20th International Conference
ENGINEERING MECHANICS 2014
Svratka, Czech Republic, 12 – 15 May 2014

INFLUENCE OF PROPELLER BLADE FORCE SPANWISE DISTRIBUTION ON WHIRL FLUTTER CHARACTERISTICS

J. Čečrdle*

Abstract: *This paper is focused on the influence of the propeller blade lift spanwise distribution on whirl flutter stability. It gives the theoretical background of the whirl flutter phenomenon and the propeller blade forces solution. The problem is demonstrated on the example of a twin turboprop aircraft structure. The influences on the propeller aerodynamic derivatives and the influences on the whirl flutter speed and the whirl flutter margin respectively are evaluated.*

Keywords: Aeroelasticity, Flutter, Propeller blade force, Whirl flutter.

1. Introduction

Whirl flutter is the specific case of the flutter that includes additional dynamic and aerodynamic influences of propeller and engine rotating parts. Effect of a rotating mass increases the number of degrees of freedom and causes additional forces and moments. Moreover, rotating propeller causes a complicated flow field and interference effects between wing, nacelle and propeller. The essential fact is an unsymmetric distribution of forces on a transversely vibrating propeller. Whirl flutter may cause a propeller mounting unstable vibrations, even a failure of an engine, nacelle or whole wing.

2. Theoretical Background

The fundamental solution presented by Reed (1967) is derived for the system with 2 degrees of freedom as illustrated in Fig. 1. Engine system flexible mounting can be substituted by the system of two rotational springs (K_Ψ, K_Θ). Propeller is considered as rigid, rotating with angular velocity Ω. System is exposed to the airflow of velocity V_∞.

Neglecting the propeller rotation and the aerodynamic forces, the two independent mode shapes will emerge with angular frequencies ω_Ψ and ω_Θ. Considering the propeller rotation, the gyroscopic effect makes two independent mode shapes merge to the whirl motion. The propeller axis shows an elliptical movement. The orientation is backward relative to the propeller rotation for the mode with lower frequency (backward whirl) and forward relative to the propeller rotation for the mode with higher frequency (forward whirl). The mode shapes of gyroscopic modes are complex, since independent yaw and pitch modes have a phase shift 90°. Gyroscopic mode shapes cause harmonic changes of propeller blades angles of attack. They give rise to unsteady aerodynamic forces, which may under the specific conditions induce whirl flutter. Provided that the air velocity is lower than critical value ($V_\infty < V_{FL}$), the system is stable and the motion is damped. If the airspeed exceeds the critical value ($V_\infty > V_{FL}$), the system becomes unstable and motion is diverging. The state of the neutral stability

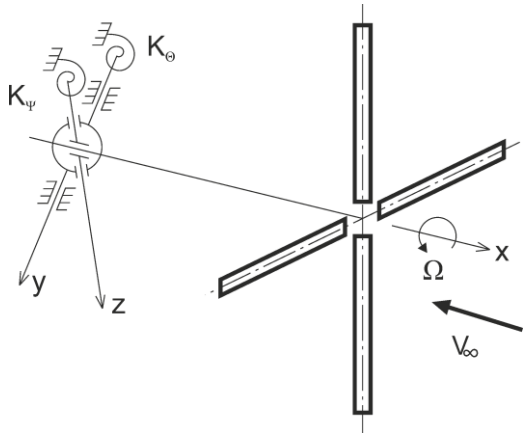

Fig. 1: Gyroscopic system with propeller.

* Ing. Jiří Čečrdle, PhD.: Strength of Structures Dept., Aeronautical Research and Test Institute (VZLU), Beranovych 130; 199 05, Prague - Letnany; CZ, cecrdle@vzlu.cz

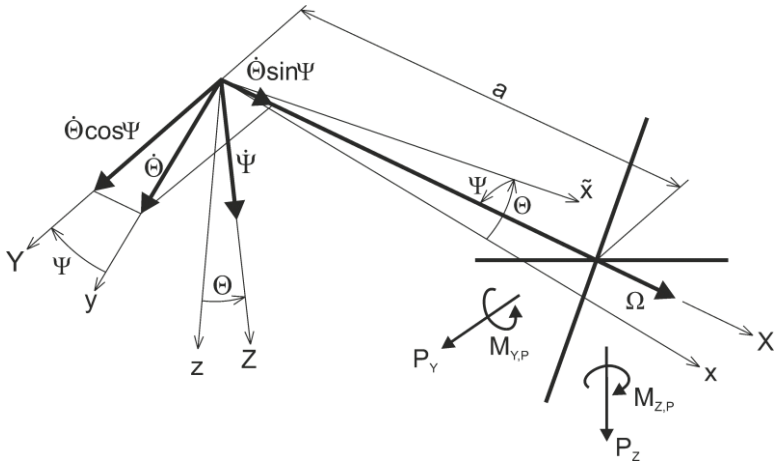

Fig. 2: Kinematical scheme of the gyroscopic system.

($\boldsymbol{V_\infty = V_{FL}}$) with no total damping is called critical flutter state and $\boldsymbol{V_{FL}}$ is called critical flutter speed.

Basic problem consists in the determination of the aerodynamic forces caused by the gyroscopic motion for the specific propeller blades. The kinematical scheme including gyroscopic effects according Reed and Bland (1961) is shown in Fig. 2. The independent generalized coordinates are three angles ($\boldsymbol{\varphi}$, $\boldsymbol{\Theta}$, $\boldsymbol{\Psi}$). We assume the propeller angular velocity constant ($\boldsymbol{\varphi = \Omega\, t}$), mass distribution symmetric around X-axis and mass moments of inertia $\boldsymbol{J_Z \neq J_Y}$. Considering small angles the equations of motion become:

$$\begin{aligned} J_Y\ddot{\Theta} + \frac{K_\Theta \gamma_\Theta}{\omega}\dot{\Theta} + J_X \Omega\dot{\Psi} + K_\Theta \Theta &= M_{Y,P} - a.P_Z \\ J_Z\ddot{\Psi} + \frac{K_\Psi \gamma_\Psi}{\omega}\dot{\Psi} - J_X \Omega\dot{\Theta} + K_\Psi \Psi &= M_{Z,P} + a.P_Y \end{aligned} \tag{1}$$

We formulate the propeller aerodynamic forces by means of the aerodynamic derivatives as described later and make the simplification for the harmonic motion. Then the final whirl flutter matrix equation become:

$$\left(-\omega^2[M] + j\omega\left([D]+[G]+q_\infty F_P \frac{D_P^2}{V_\infty}[D^A]\right)+\left([K]+q_\infty F_P D_P[K^A]\right)\right)\begin{bmatrix}\overline{\Theta}\\ \overline{\Psi}\end{bmatrix} = \{0\} \tag{2}$$

The limit state emerges for the specific combination of parameters $\boldsymbol{V_\infty}$ and $\boldsymbol{\Omega}$, when the angular velocity $\boldsymbol{\omega}$ is real. Whirl flutter appears at the gyroscopic rotational vibrations, the flutter frequency is the same as the frequency of the backward gyroscopic mode. The most critical state is $\boldsymbol{K_\Theta = K_\Psi}$, it means $\boldsymbol{\omega_\Theta = \omega_\Psi}$, when the interaction of both independent motions is maximal.

The fundamental solution of the propeller aerodynamic forces was derived by Ribner (1945). Later on, the modified solution of Houbolt and Reed (1962) became available as well. The propeller aerodynamic forces are expressed as:

$$\begin{aligned} P_Y &= \pi\,\rho V_\infty^2 R^2\left(c_{y\Theta}\Theta^* + c_{y\Psi}\Psi^* + c_{yq}\frac{\dot{\Theta}^* R}{V_\infty} + c_{yr}\frac{\dot{\Psi}^* R}{V_\infty}\right) \\ P_Z &= \pi\,\rho V_\infty^2 R^2\left(c_{z\Theta}\Theta^* + c_{z\Psi}\Psi^* + c_{zq}\frac{\dot{\Theta}^* R}{V_\infty} + c_{zr}\frac{\dot{\Psi}^* R}{V_\infty}\right) \\ M_{Y,P} &= 2\pi\,\rho V_\infty^2 R^3\left(c_{m\Theta}\Theta^* + c_{m\Psi}\Psi^* + c_{mq}\frac{\dot{\Theta}^* R}{V_\infty} + c_{mr}\frac{\dot{\Psi}^* R}{V_\infty}\right) \\ M_{Z,P} &= 2\pi\,\rho V_\infty^2 R^3\left(c_{n\Theta}\Theta^* + c_{n\Psi}\Psi^* + c_{nq}\frac{\dot{\Theta}^* R}{V_\infty} + c_{nr}\frac{\dot{\Psi}^* R}{V_\infty}\right) \end{aligned} \tag{3}$$

where $\boldsymbol{\rho}$ is a dynamic pressure and $\boldsymbol{R}$ is a propeller diameter. The effective angles ($\boldsymbol{\Theta^*; \Psi^*}$) are basically expressed as the quasi-steady values (($\boldsymbol{\Theta^* = \Theta + (\dot{Z}/V_\infty)}$); ($\boldsymbol{\Psi^* = \Psi - (\dot{Y}/V_\infty)}$)) and the $\boldsymbol{c_{ij}}$ terms represent the aerodynamic derivatives. We neglect the aerodynamic inertia terms ($\boldsymbol{\dot{\Theta}^* \approx \dot{\Theta}}$; $\boldsymbol{\dot{\Psi}^* \approx \dot{\Psi}}$), make the simplification given by the symmetry ($\boldsymbol{c_{z\Psi} = c_{y\Theta}}$; $\boldsymbol{c_{m\Psi} = -c_{n\Theta}}$; $\boldsymbol{c_{mq} = c_{nr}}$; $\boldsymbol{c_{zr} = c_{yq}}$; $\boldsymbol{c_{z\Theta} = -c_{y\Psi}}$; $\boldsymbol{c_{n\Psi} = c_{m\Theta}}$; $\boldsymbol{c_{mr} = -c_{nq}}$; $\boldsymbol{c_{yr} = -c_{zq}}$) and we neglect the derivatives with low values ($\boldsymbol{c_{mr} = -c_{nq} = 0}$; $\boldsymbol{c_{yr} = -c_{zq} = 0}$). As the result, we obtain 6 independent values of aerodynamic derivatives expressed by the propeller blade integrals that integrate the aerodynamic forces in the blade spanwise direction.

The basic formulation was given by Houbolt and Reed (1962). It is limited to the 4-blade propeller and theoretical blade lift curve slope ($a_0 = 2\pi$). It includes only 3 integrals accounting for the in-phase aerodynamic effects. Extended formulation of the blade integrals is presented by Rodden and Rose (1989). It includes the aerodynamic lift lag effect by means of the Theodorsen function ($F(k_p)+jG(k_p)$), the Prandtl - Glauert correction to the compressibility and the correction factor accounting for the compressible flow blade aspect - ratio effect. Final correction is applied to account for the number of blades. Integration range is reduced to the thrusting part of the propeller. The propeller lift curve slope (a_0) is treated as the effective (spanwise constant) value ($a_0 = a_{0eff}$). Contrary to Rodden's formulation, we use more precise approach, that treats the lift curve slope as the spanwise variable ($a_0 = a_0(\eta)$) accounting for the real propeller force distribution. In this case a_0 moves under the integrand and the propeller blade integrals become:

$$
\begin{aligned}
I_1 &= \left(\frac{N_b}{4}\right)\left(\frac{1}{2\pi}\right)\frac{\mu^2 A_r}{c_r}\int_{\eta_0}^{1}\frac{a_0(\eta)c(\eta)F(k_P)}{\sqrt{\mu^2+\eta^2}\left[2+A_r\sqrt{1-M^2\left(1+\frac{\eta^2}{\mu^2}\right)}\right]}d\eta \\
J_1 &= \left(\frac{N_b}{4}\right)\left(\frac{1}{2\pi}\right)\frac{\mu^2 A_r}{c_r}\int_{\eta_0}^{1}\frac{a_0(\eta)c(\eta)G(k_P)}{\sqrt{\mu^2+\eta^2}\left[2+A_r\sqrt{1-M^2\left(1+\frac{\eta^2}{\mu^2}\right)}\right]}d\eta \\
I_2 &= \left(\frac{N_b}{4}\right)\left(\frac{1}{2\pi}\right)\frac{\mu A_r}{c_r}\int_{\eta_0}^{1}\frac{\eta^2 a_0(\eta)c(\eta)F(k_P)}{\sqrt{\mu^2+\eta^2}\left[2+A_r\sqrt{1-M^2\left(1+\frac{\eta^2}{\mu^2}\right)}\right]}d\eta \\
J_2 &= \left(\frac{N_b}{4}\right)\left(\frac{1}{2\pi}\right)\frac{\mu A_r}{c_r}\int_{\eta_0}^{1}\frac{\eta^2 a_0(\eta)c(\eta)G(k_P)}{\sqrt{\mu^2+\eta^2}\left[2+A_r\sqrt{1-M^2\left(1+\frac{\eta^2}{\mu^2}\right)}\right]}d\eta \\
I_3 &= \left(\frac{N_b}{4}\right)\left(\frac{1}{2\pi}\right)\frac{A_r}{c_r}\int_{\eta_0}^{1}\frac{\eta^4 a_0(\eta)c(\eta)F(k_P)}{\sqrt{\mu^2+\eta^2}\left[2+A_r\sqrt{1-M^2\left(1+\frac{\eta^2}{\mu^2}\right)}\right]}d\eta \\
J_3 &= \left(\frac{N_b}{4}\right)\left(\frac{1}{2\pi}\right)\frac{A_r}{c_r}\int_{\eta_0}^{1}\frac{\eta^4 a_0(\eta)c(\eta)G(k_P)}{\sqrt{\mu^2+\eta^2}\left[2+A_r\sqrt{1-M^2\left(1+\frac{\eta^2}{\mu^2}\right)}\right]}d\eta
\end{aligned}
\tag{4}
$$

where A_r is a blade aspect ratio, c is a blade local chord, k_p is a blade local reduced frequency. A propeller advance ratio is defined as $\mu = (V_\infty/\Omega R)$ and a blade dimensionless radius is defined as $\eta = (r/R)$ where r is a blade local radius. M represent the forward flow Mach number. Aerodynamic derivatives are then expressed as:

$$
\begin{aligned}
c_{z\Theta} &= -\left(\frac{4\Omega c_r}{V_\infty}\right)I_1 \;\; ; \;\; c_{zq} = \left(\frac{4\Omega c_r}{V_\infty}\right)J_2 \;\; ; \;\; c_{m\Theta} = -\left(\frac{2\Omega c_r}{V_\infty}\right)J_2 \;\; ; \;\; c_{mq} = -\left(\frac{2\Omega c_r}{V_\infty}\right)I_3 \\
c_{y\Theta} &= -\left(\frac{4\Omega c_r}{V_\infty}\right)J_1 \;\; ; \;\; c_{yq} = -\left(\frac{4\Omega c_r}{V_\infty}\right)I_2 \;\; ; \;\; c_{n\Theta} = -\left(\frac{2\Omega c_r}{V_\infty}\right)I_2 \;\; ; \;\; c_{nq} = -\left(\frac{2\Omega c_r}{V_\infty}\right)J_3
\end{aligned}
\tag{5}
$$

3. Application Example

The evaluation is performed on the structure of the **EV-55M** aircraft that is ordinary twin turboprop for ***9 - 13*** passengers powered by **PT6A-21** turboprop engines with Avia **AV-844** propellers. Firstly, the evaluation of the aerodynamic derivatives is provided. The blade lift curve slope spanwise distribution as well as the geometry of the blade cannot be reproduced here. The effective value extracted by means of the ***RMS*** method of $a_{0eff} = 6.2478$ is slightly lower comparing to the profile theoretical value of 2π.

Fig. 3 shows the example of aerodynamic derivative dependence on the flow velocity considering both a_{0eff} and $a_0(\eta)$. The derivative values considering $a_0(\eta)$ are lower comparing to the ones using a_{0eff}. This fact hold true also for the other ones which are not shown here.

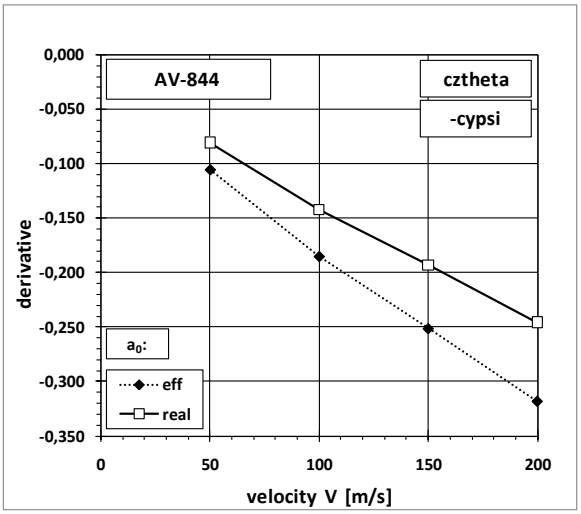

Fig. 3: Aerodynamic derivative $c_{z\Theta}$ - blade lift slope: a_{0eff} ; $a_0(\eta)$.

The final evaluation of the whirl flutter speed was performed using the **NASTRAN** program system supported by the in-house **PROPFM** software code. The effective stiffnesses of the engine mount in both vertical and lateral directions were reduced by ***50%*** to reach the critical state within the reasonable velocity range wherever the standard analytical approach was employed. The results indicate the backward whirl flutter on the mode ***#2*** that is the engine vertical vibrations mode. The flutter speed is $\mathbf{V_{FL} = 166.6\ [m.s^{-1}]}$ considering the effective value of the lift curve slope, whereas the flutter speed become $\boldsymbol{V_{FL} = 182.0\ [m.s^{-1}]}$ considering the real lift curve slope distribution. It represents the increase in the flutter speed by ***9.2%***. The flutter frequency was $\boldsymbol{f_{FL} = 5.8\ [Hz]}$, the difference between both cases was barely noticeable.

Further explanation of the blade lift slope influence to the whirl flutter characteristics is provided in Fig. 4. It shows the stability margin defining the critical values of the structural parameters (e.g. vertical and lateral engine vibration mode frequencies) required to reach the neutral stability at the certain speed. Again, the real distribution of the lift curve slope gives the lower critical frequencies and thus higher reserve in terms of the whirl flutter stability with respect to the nominal state. The differences between both margins are ranging within **(5.5 - 7.1)%.**

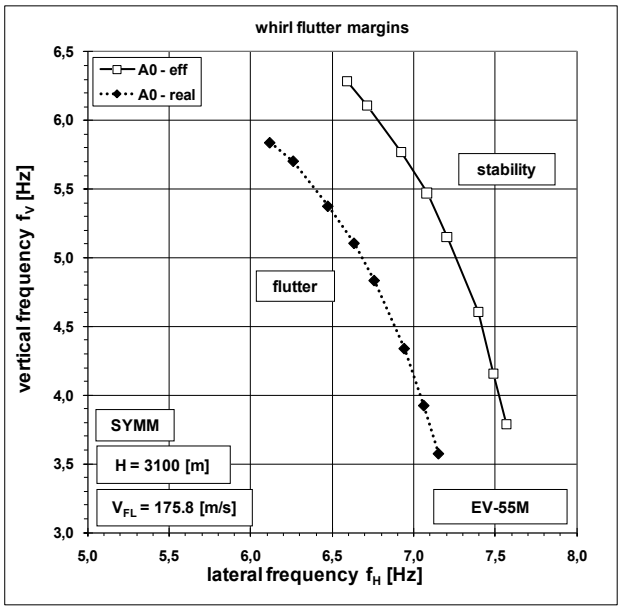

Fig. 4: Whirl flutter stability margins - blade lift slope: a_{0eff} ; $a_0(\eta)$.

4. Conclusion

Usage of the real propeller blade lift curve slope distribution increases the accuracy of results and raises the rate of reserve in terms of flutter stability. It causes decrease of the aerodynamic derivatives and, as the consequence, it increase the flutter speed and decrease the critical values of the structural parameters. Comparing to the usage of the effective value the derivatives may vary quite significantly.

References

Ribner, H.S. (1945) Propellers in Yaw, NASA Rep. 820.

Reed, W.H. & Bland, S.R. (1961) An Analytical Treatment of Aircraft Propeller Precession Instability, NASA, Technical Note, TN D-659.

Houbolt, J.C & Reed, W.H. (1962) Propeller Nacelle Whirl Flutter, Journal of Aerospace Sciences, Vol.29, March 1962, pp. 333-346.

Reed, W.H. (1967) Review of Propeller - Rotor Whirl Flutter, NASA Technical Report, TR R-264.

Rodden, W.P. & Rose, T.L. (1989) Propeller / Nacelle Whirl Flutter Addition to MSC/NASTRAN, MSC World User's Conference, Universal City, CA, USA.